FINITE ELEMENT ANALYSES OF A LAMINATED BLADE RETENTION SYSTEM

Dennis K. McCarthy **Robert T. Fort**

McDonnell Douglas Helicopter Systems
5000 East McDowell
Mesa, Arizona 85215

ABSTRACT

Design of a helicopter main rotor blade retention system is a challenging problem. This critical system must reliably carry large blade loads while allowing extreme blade motions. Several different methods for blade retention systems are currently in service including laminated metallic stacks (LMS). Due to the lack of precise analytic methods laminated metallic stack systems have historically been developed through test. A methodology, developed by the authors, is presented herein to accurately predict the behavior of a LMS blade retention system. This method uses nonlinear finite element (FE) analysis to predict LMS motions and stresses. Finite element results are interrogated to obtain damage and fatigue life predictions. The analytical results are compared to test data with excellent agreement thus verifying the methodology.

INTRODUCTION

The main rotor blade retention system on a helicopter presents a particularly difficult design and analysis problem. The system must be sufficiently robust to resist the high centrifugal and shear (drag) forces imparted by the rotor blade yet be sufficiently compliant to accommodate the large out-of-plane feather and flapping motions required to provide lift to the aircraft. This problem is further aggravated with increased aircraft weight since this results in higher centrifugal and shear forces while still requiring the large feather and flap angles necessary for controlled flight.

Design approaches to carry blade forces and accommodate blade motion currently in use include: 1) Fully articulated systems with bearings for each degree of freedom. 2) Composite flexible beams, 3) elastomeric bearings, and 4) Laminated metallic stacks (LMS).

Construction of the main rotor head of a typical light helicopter with the LMS highlighted is shown in Figure 1. The LMS, shown in Figure 2, is composed of 16 bifurcated stainless steel laminae. The laminae are 0.009" thick and are separated from each other by thin stainless steel shims at the outboard and inboard ends. The inboard ends are bolted to the main rotor hub. The single outboard end is sandwiched between two shoes and is attached to the root end of the blade though a lead-lag link. In this configuration centrifugal and shear forces imparted by the blade are carried through the laminae to the hub. Feathering is a pilot control input which increases blade pitch resulting in aerodynamic lift. This lift results in a blade flapping motion which wraps the LMS around the main rotor hub. This in turn provides the necessary vertical shear force on the hub to lift the aircraft. The LMS accommodates flapping and feathering by relative motion between the laminae.

The nonlinear behavior of the LMS with its axial stiffening, large displacements, and complex buckling modes makes it an extremely difficult problem to solve analytically. Historically, stresses in an LMS have been determined primarily through laboratory and flight testing which is a time consuming and costly method to develop new designs. The preferred development method is to analytically optimize the design prior to any testing. A method to predict LMS motions, stresses, and fatigue life has been developed by the authors and is summarized in this paper.

The method requires three nonlinear finite element models to accurately predict lamina stresses. First loads and motions are applied to a coarse mesh model of the entire LMS assembly. Displacements and internal forces are recovered for critical lamina. These displacements are then applied to a refined single lamina model to obtain detailed stresses. Similarly a third refined nonlinear model of the outboard (bolted) end predicts stresses for this region of the LMS assembly.

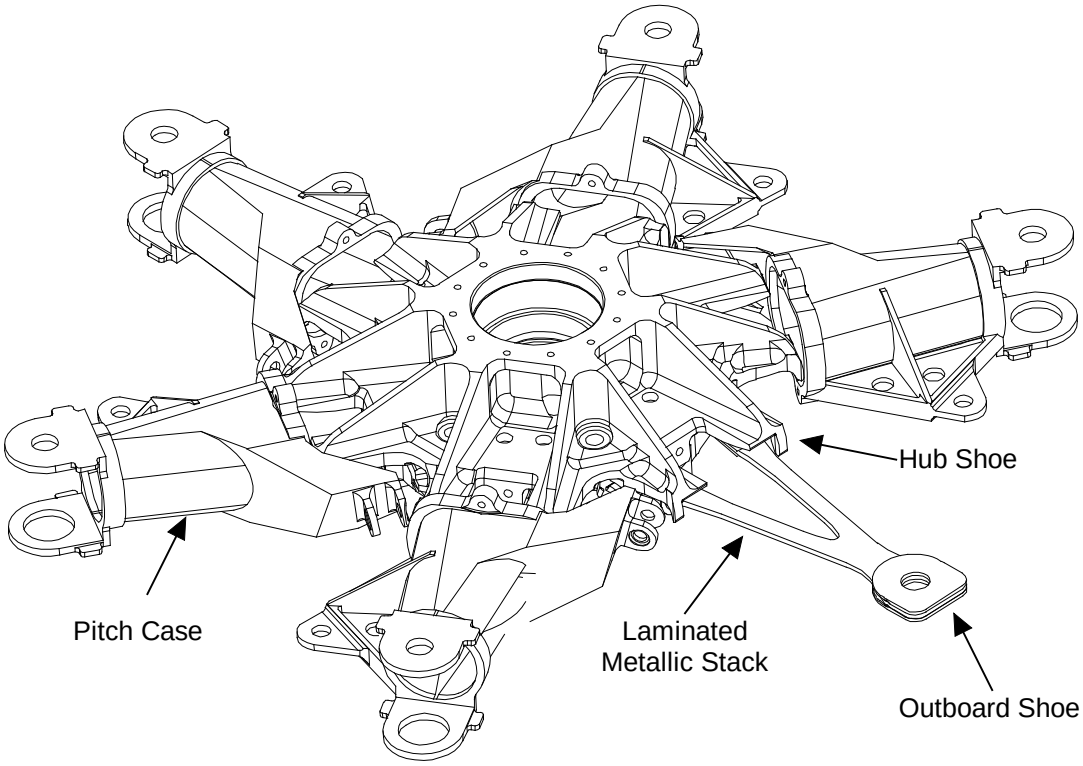

Figure 1. Typical Light Helicopter Main Rotor Hub.

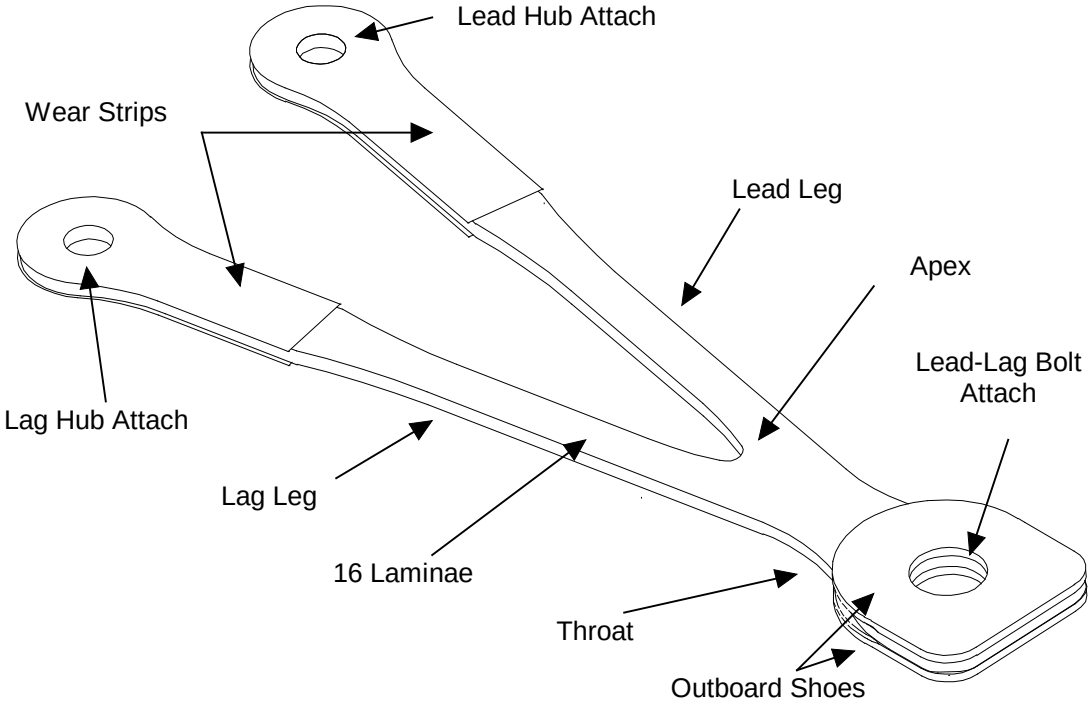

Figure 2. Typical Light Helicopter Laminated Metallic Stack.

Grid point stresses are extracted from the two refined models for each data point within a maneuver. These stresses are used to calculate maximum, minimum, and Goodman corrected cyclic stresses for each maneuver. The corrected stresses are then compared to material S-N data to calculate the damage per maneuver. Using Minor's rule these damages are summed over a flight spectrum to obtain a predicted part life.

In the case of initial or redesign of an LMS the procedure is repeated to optimize the lamina geometry that will result in the longest fatigue life within the aircraft's constraints.

MATERIAL PROPERTIES

LMS laminae are typically machined from stainless steel sheet. Properties for 17-4 PH stainless steel sheet shown in Table 1 [1] were used for this analysis.

Table 1. 17-4 PH Stainless Steel Sheet Properties

Property	units	17-4 PH
Young's Modulus	msi	28.5
Shear Modulus	msi	11.2
Poisson's Ratio	msi	0.27
Yield Strength	ksi	170
Ultimate Strength	ksi	190

Figure 3 shows fatigue behavior of 17-4 stainless steel for an (R) value of 0.1 [2]. Where (R) is defined as

$$R = \frac{\sigma_{min}}{\sigma_{max}}$$

Also shown is the cyclic stress Goodman corrected to an 85 ksi mean stress using

$$\sigma_G = \sigma_{cyc} \cdot \left(\frac{\sigma_{ult} - \sigma_{mvl}}{\sigma_{ult} - \sigma_{mean}} \right)$$

where σ_{mvl} is the mean stress for Goodman correction (σ_{mvl}=85 ksi)
σ_{ult} is the ultimate strength (σ_{ult}=190 ksi)

LOADS

The laminated metallic stack attaches the main rotor blades to the hub. The LMS resists rotor blade centrifugal and tangential forces while allowing feathering and flapping motion. These loads and motions are shown in Figure 4.

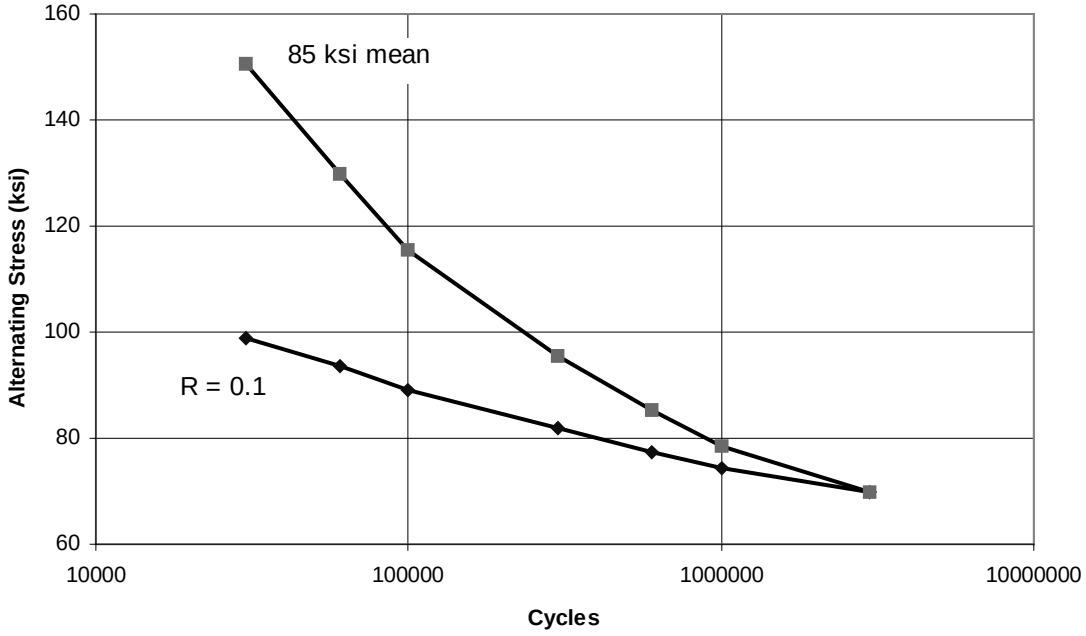

Figure 3. 17-4 PH Stainless Steel Bar S-N Behavior.

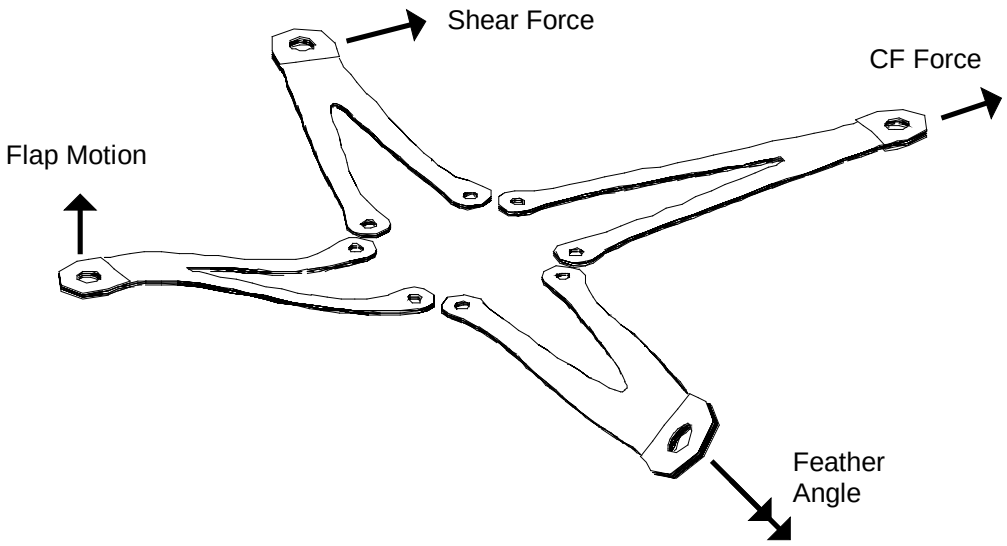

Figure 4. LMS Loads and Displacements.

Blade centrifugal force (CF) is the dominant load. Aerodynamic drag and inertial lead-lag blade motion result in chordwise shear force. These forces are carried to the hub via the "truss" arrangement formed by the LMS.

Blade feathering is a pitch change controlled by the pilot. An elastomeric mount provides the pivot for this motion. The pitch case rotates about this mount and in turn rotates the LMS about its longitudinal axis.

Blade flapping is the means by which blade lift is transmitted to the rotor hub. As more lift is generated the blades cone up rotating the pitch case about the tangential axis of the elastomeric mount. Coning causes the LMS to wrap around the hub shoe on the rotor thus lifting the ship.

The spectrum shown in Table 2 is used to demonstrate the analysis method. This spectrum contains four maneuvers and their number of occurrences per 10 hour block.

Table 2. Sample Maneuver Spectrum

Maneuver	**Cycles per 10 hour block**
High Speed Level Flight	175000
Right Turn	300
High G Rolling Pull Out	35
High G Symmetric Pull Up	40

Six data points for each maneuver corresponding to maximum and minimum flap, feather, and shear were considered. CF, shear, flap, and feather for each of the six data points during each of the four maneuvers are shown in Table 3.

Table 3. Sample Spectrum Maneuver Loads*

Maneuver	Condition	cf (lbs)	shear (lbs)	flap degree	feather degree
Level Flight	Min Flap	87%	12%	29%	83%
	Max Flap	86%	47%	48%	-5%
	Min Feather	86%	49%	48%	-5%
	Max Feather	87%	11%	29%	83%
	Min Shear	88%	5%	32%	73%
	Max Shear	84%	54%	45%	-5%
Right Turn	Min Flap	83%	9%	18%	69%
	Max Flap	89%	47%	82%	-12%
	Min Feather	85%	75%	75%	-25%
	Max Feather	87%	-18%	25%	81%
	Min Shear	90%	-26%	39%	74%
	Max Shear	82%	82%	61%	-18%
RPO	Min Flap	70%	3%	-3%	29%
	Max Flap	84%	33%	99%	-36%
	Min Feather	77%	87%	82%	-53%
	Max Feather	77%	-52%	16%	47%
	Min Shear	82%	-62%	39%	40%
	Max Shear	73%	99%	57%	-47%
Pull Up	Min Flap	76%	15%	12%	-14%
	Max Flap	93%	42%	81%	59%
	Min Feather	83%	83%	29%	-52%
	Max Feather	86%	-27%	63%	98%
	Min Shear	80%	-44%	40%	80%
	Max Shear	89%	100%	52%	-34%

* Loads are normalized to protect information proprietary to MDHS.

ANALYSIS METHODOLOGY OVERVIEW

Understanding and predicting the highly nonlinear behavior of a laminated metallic stack involves several detailed steps as outlined by the flow chart in Figure 5. Critical loads from each maneuver that define the aircraft's usage are applied to a coarse multi lamina finite element model.

Boundary displacements are extracted from the multi lamina results and applied to refined models of individual lamina for detailed stress evaluation. In a similar manner, stresses in the outboard joint region are determined. A refined finite element model of the joint is subjected to boundary forces and displacements derived from the multi lamina analysis.

Nodal stresses from the refined mesh models are then interrogated to determine cyclic and mean stresses for each maneuver. These stresses are Goodman corrected and a resulting maneuver damage is determined employing an S-N curve. The damage for each maneuver is summed using Minor's Rule for the aircraft's usage spectrum. The resulting value of cumulative damage is used to derive the life of the LMS. Lamina geometry can then be modified to lower stresses and the procedure repeated until the design is optimized.

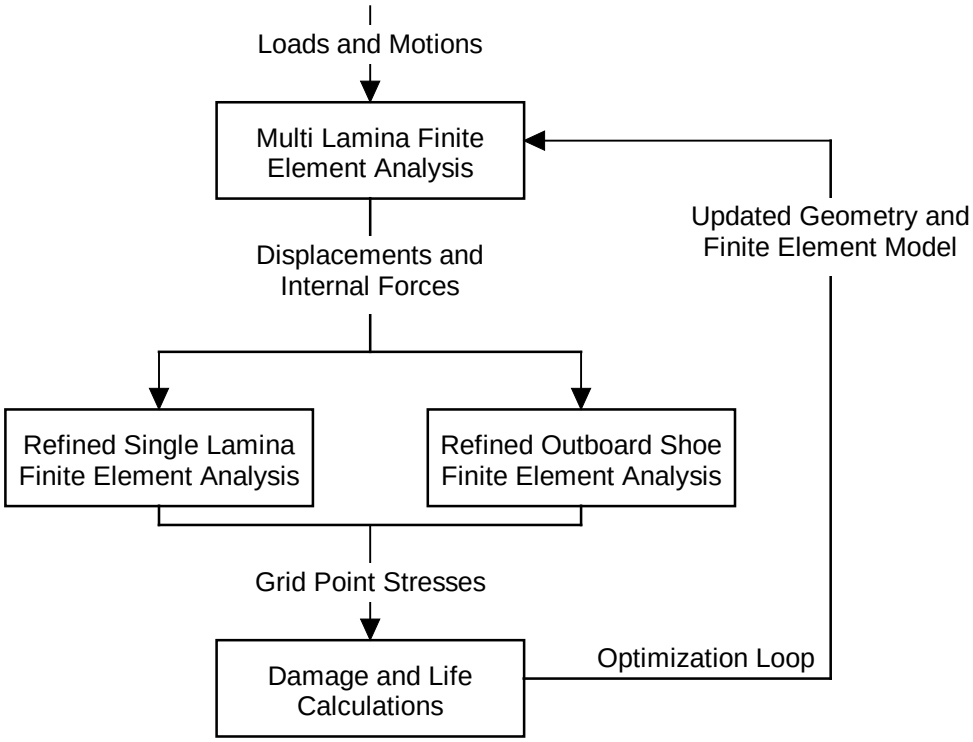

Figure 5. LMS Analysis Methodology Flowchart

.

NONLINEAR FINITE ELEMENT ANALYSES

The finite element analyses of the laminated metallic stack presented in this paper were accomplished using MSC/PATRAN as a model generation tool and MSC/NASTRAN finite element code as a solver. Due to the highly nonlinear behavior of the LMS, NASTRAN Solution 106 was used for **all** analyses. These analyses were run on a HP 735 work station.

Non-linear effects that were accounted for in the analyses included:

1. Large displacements required to flap and feather the LMS during rotor operation.

2. Axial stiffening of the laminae due to the applied centrifugal force.

3. Varying contact forces at component interfaces as a result of relative motions between components.

A nonlinear analysis requires substantially more computer time and produces a great deal more output as a similar size linear analysis. Therefore it was necessary to minimize the size of the multi lamina FE model. This reduction sacrificed accuracy in critical regions such as the apex where four elements define its geometry. More accurate stress evaluation for areas such as the apex and throat were achieved by applying deformations and/or forces from any of the lamina of the coarse model to a refined single lamina and outboard shoe models. This procedure is discussed in detail in the following sections.

The order of load and motion application is very important for this analysis to insure rapid solution convergence. Extensive study by the authors on LMS behavior has shown that the following load application sequence leads to the fastest convergence on a particular load case. The loads and motions are applied incrementally in the following order:

1. CF is applied in one load increment. The CF load stabilizes the laminae and prevents unrealistic buckling upon application of other loads and motions.

2. The lower hub shoe is bolted to the upper vertically displacing the inboard legs to form the build condition. This is simulated in one load increment by displacing the inboard legs.

3. Shear force is applied to the outboard end in one load increment.

4. Feathering of the model normally can be accomplished with one load increment. Larger angles (> 15 degrees) require a few increments. This is due to the changes in contact area and forces of the laminae on the hub shoes.

5. Flap is applied last. Application of the flap angle reduces the axial force in the upper laminae. This reduction combined with high shear forces initiates buckling in upper laminae trailing legs at flap angles as low as 8 degrees. This buckling greatly aggravates convergence of the analysis resulting in extremely long compute times or divergence of the solution. As a result several smaller angle increments (approximately 0.5 degrees) are required to allow convergence.

MULTI LAMINA FINITE ELEMENT MODEL

The multi lamina model as shown in Figure 6 includes the LMS, pitch case, lead-lag link, elastomeric mount, hub shoes, and striker plate. The laminae are composed of coarsely meshed quadrilateral shell elements positioned at the true centerlines of the LMS (separation due to inboard and outboard shims as well as lamina thickness is accounted for). The inboard ends of the legs were fixed in all directions under the bolt footprint except for the vertical direction. This allows for input of the vertical displacement that simulates build.

Stiff vertical springs provide the contact points between successive laminae at the inboard and outboard ends. Gap elements were used between the top and bottom laminae to simulate the upper and lower hub shoe contours. One end of the gap element was attached to the lamina surface while the other end was grounded. The initial gap opening for each element was set equal to the vertical distance between the LMS in its neutral position to the appropriate hub shoe.

The outboard shoes were modeled using quadrilateral shell elements. The shoes and each lamina make use of a series of stiff beam elements in a spoke arrangement to mimic the outboard bolt. Stiff beam elements tie the laminae and shoes together in the vertical direction to complete the bolt representation.

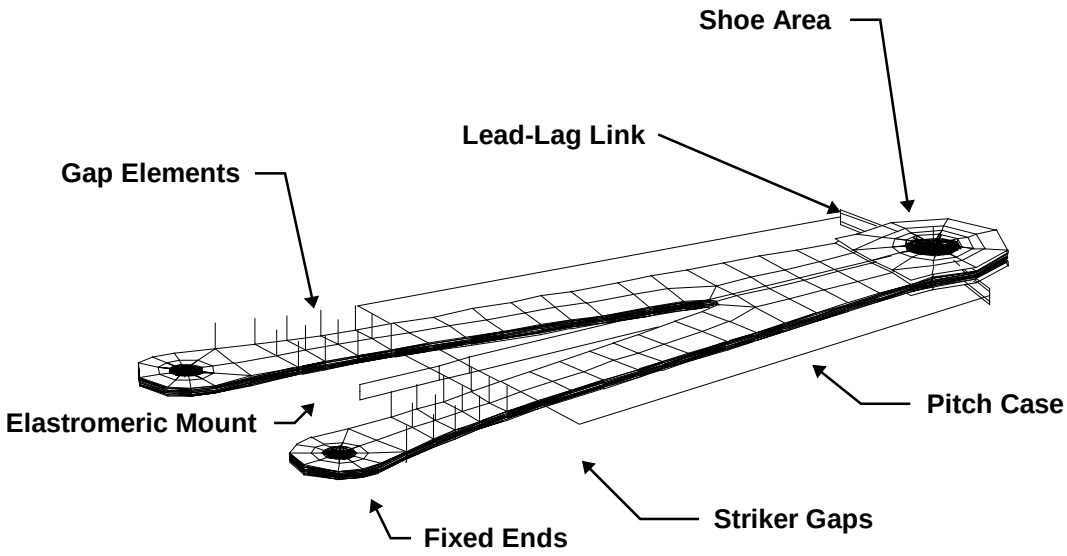

Figure 6. LMS Multi Lamina Finite Element Model.

The pitch case was modeled using stiff beam elements. The outboard end was rigidly attached to the upper and lower ends of the simulated bolt. The ends of the two beams extending laterally from the pitch case represent the striker plate. At each end of the striker plate a single gap element to ground represents the initial clearance between the striker plate and the hub. Closure of one of these gaps results in another load path through the pitch case. The inboard end of the pitch case model is attached to six grounded spring elements that represent the stiffness of the elastomeric mount for all six degrees of freedom.

The lead-lag link was modeled with stiff beam elements attached to the outboard bolt by two translational springs at four separate locations. An additional vertical spring was attached to prevent rigid body motion. This arrangement allowed the link to rotate about the bolt thus simulating actual lead-lag link motion.

Centrifugal and chord shear forces were distributed to the center nodes on each laminas outboard end. To simulate the inboard build condition the inboard bolts that attach the laminae to the hub are displaced vertically causing an interference between the LMS and the upper hub shoe as simulated by the gap elements.

Flap and feather motions are applied to the outboard end by displacing a pair of nodes on either side of the outboard hole at the LMS center line. Equal and opposite displacement in the vertical direction simulates feather motion and equal vertical displacement simulates flapping motion. The two motions can be combined to account for any possible flight condition.

REFINED SINGLE LAMINA FE MODEL

The refined quadrilateral shell mesh, shown in Figure 7, was created to determine stresses in the critical top and bottom laminae of the LMS.

Displacements are extracted from multi-lamina finite element results files and applied to the refined mesh at the interfaces shown in Figure 8. An interpolation program is used to account for the different mesh densities between the coarse and fine meshes. Stresses are then used to calculate laminae damage.

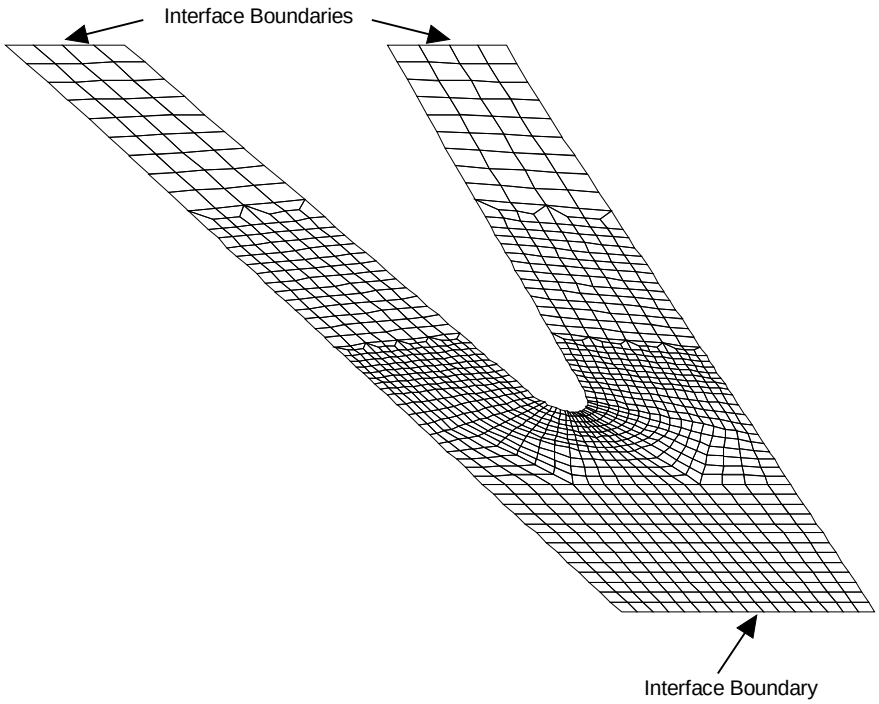

Figure 7. Refined Single Lamina Finite Element Mesh.

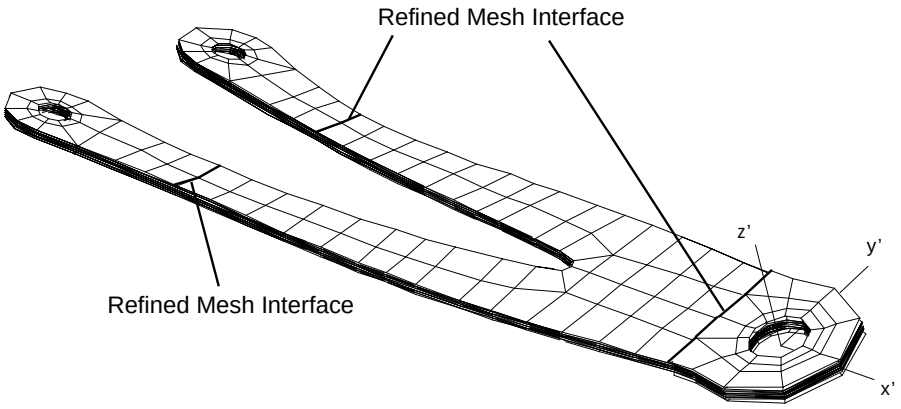

Figure 8. Refined Single Lamina Finite Element Model Interface Locations.

OUTBOARD SHOE FINITE ELEMENT MODEL

The refined finite element mesh shown in Figure 9 was used to model the behavior of the outboard joint of the LMS. The shoes and top and bottom laminae were modeled using quadrilateral shell elements. Vertical springs separate the top and bottom laminae as well as the lamina to shoe interface in the shim area. Vertical beams simulate the lead-lag bolt and radial beams simulate load transfer between the bolt, laminae, and shoes.

Interface loads and motions for the top and bottom laminae were extracted from results of the multi lamina FE analysis. Motions include vertical displacements and feathering and flapping rotations. Loads include axial and lateral forces and yawing moments. These loads and motions were read from the NASTRAN results files and transformed to the displaced coordinate system shown in Figure 10. Stresses were then extracted to determine lamina throat damage as detailed in the next section.

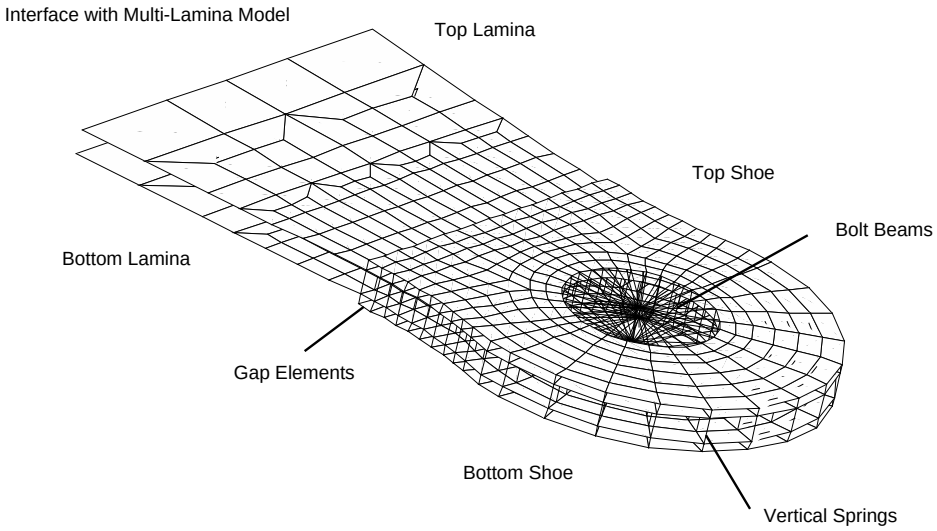

Figure 9. Outboard Shoe Finite Element Mesh.

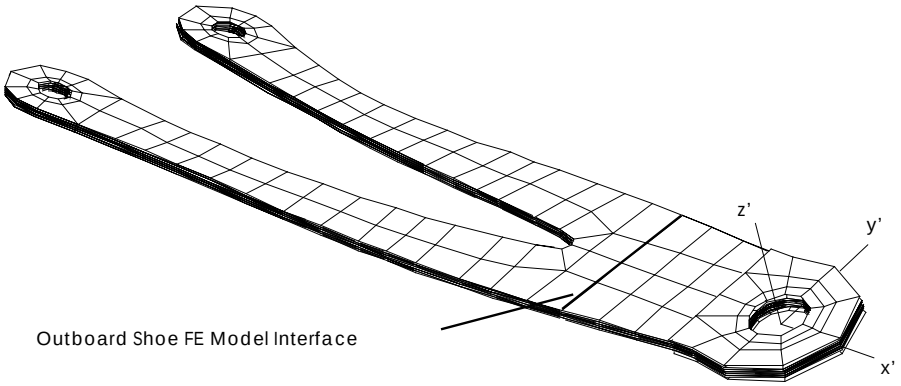

Figure 10. Refined Outboard Shoe Finite Element Model Interface Location.

DAMAGE AND FATIGUE

A method was developed to calculate fatigue life from NASTRAN finite element results. Grid point stresses are obtained from PATRAN binary result files. The stress state (σ_x, σ_y, and τ_{xy}; top and bottom) is stored for each node and load within a maneuver. Typically, six data points are sufficient to define maneuver stress extremes: maximum and minimum flap, feather, and shear. A differential stress state (σ_d) is defined between two data points within a maneuver as

$$\sigma_d = \sigma_i - \sigma_j$$

where σ_i, σ_j are the stress state at a node for loads i and j, respectively

Average, maximum shear, and maximum and minimum principal stresses (σ_{dave}, σ_{dms}, σ_{d1}, and σ_{d2}) are calculated for the differential stress state using

$$\sigma_{dave} = 0.5 \cdot \left(\sigma_{dx} + \sigma_{dy}\right)$$

$$\sigma_{dms} = \sqrt{\left(\frac{\sigma_{dx} - \sigma_{dy}}{2}\right)^2 + \sigma_{dxy}^2}$$

$$\sigma_{d1} = \sigma_{dave} + \sigma_{dms}$$

$$\sigma_{d2} = \sigma_{dave} - \sigma_{dms}$$

The rotation angle (θ) to transform to these principal stresses is

$$\theta = \arcsin\left(\frac{\sigma_{dxy}}{\sigma_{dms}}\right)$$

The stress states for load points within a maneuver are compared to obtain the maximum absolute differential normal stress (σ_{dmax}). This is twice the maneuver maximum cyclic stress

$$\sigma_{cyc} = \frac{\sigma_{dmax}}{2}$$

Maximum and minimum stresses (σ_{max} and σ_{min}) for that maneuver are calculated by transforming the stresses to an orientation resulting in the maximum differential stress

$$\sigma_{max} = \frac{\sigma_{1x} + \sigma_{1y}}{2} + \left(\frac{\sigma_{1x} - \sigma_{1y}}{2}\right) \cdot \cos 2\theta + \tau_{1xy} \cdot \sin 2\theta$$

$$\sigma_{min} = \frac{\sigma_{2x} - \sigma_{2y}}{2} + \frac{\sigma_{2x} - \sigma_{2y}}{2} \cdot \cos 2\theta + \tau_{2xy} \cdot \sin 2\theta$$

where σ_1, σ_2 are stresses for load points resulting in the maximum differential stress

The mean stress (σ_{mean}) is then defined as

$$\sigma_{mean} = \frac{\sigma_{max} + \sigma_{min}}{2}$$

Goodman corrected cyclic stress (σ_G) is calculated using

$$\sigma_G = \sigma_{cyc} \cdot \left(\frac{\sigma_{ult} - \sigma_{mvl}}{\sigma_{ult} - \sigma_{mean}}\right)$$

where σ_{mvl} is the mean stress for Goodman correction (σ_{mvl}=85 ksi)
σ_{ult} is the ult. strength (σ_{ult}=190 ksi)

The number of cycles to failure (N_G) corresponding to the Goodman corrected stress (σ_G) is obtained by linearly interpolating the semi log S-N data shown in Figure 11. This is calculated by

$$N_G = 10^{\left[\log N_1 + \left(\frac{S_2 - \sigma_G}{S_1 - S_2}\right) \cdot \left(\log N_1 - \log N_2\right)\right]}$$

Inverting the number of cycles to failure (N_G) yields the incremental damage for the maneuver.

$$D_i = \frac{1}{N_G}$$

The maneuvers are grouped into the spectrum shown in Table 2. Using Miner's rule the total spectrum damage ($D_{spectrum}$) becomes

$$D_{spectrum} = \sum_{i=1}^{n} D_i N_i$$

where D_i incremental maneuver damage
N_i number of maneuver occurrences
n number of maneuvers in spectrum

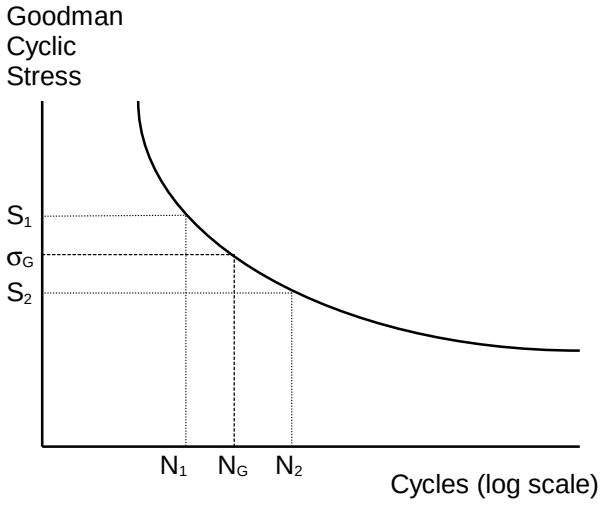

Figure 11. Semi Log S-N Data.

RESULTS

Maximum principal stress contours for a Symmetric Pull Up maneuver are shown in Figure 12. These contours are for the minimum and maximum feather conditions for the refined bottom lamina mesh. Minimum and maximum feather conditions represent the extreme stress states that define maximum cyclic stress in the trailing apex of the bottom lamina. These stress extremes of -39 ksi and 153 ksi result in a mean and cyclic stresses of 57 and 96 ksi, respectively. The stresses are Goodman corrected to an 85 ksi mean using the method outlined in the preceding damage section. The resulting maximum Goodman corrected stress for this location is 79 ksi. This stress corresponds to a damage of .0000011 per cycle. Figure 12 shows the Goodman corrected stress and damage contours for the entire region.

Similar data is shown in Figure 13 for the bottom lamina of the outboard shoe finite element model. Extremes for this location are defined by the minimum flap and maximum feather conditions. The resulting minimum and maximum stresses are shown to be 38 and 208 ksi, respectively. These result in a Goodman corrected cyclic stress of 118 ksi which corresponds to .0000155 damage per cycle.

Load points for all maneuvers for the refined single lamina and outboard shoe finite element models were automatically evaluated in a similar manner. Throat results were obtained from the outboard shoe finite element model and apex and leg results were obtained from the refined single lamina model. Mean and cyclic stresses are summarized in Tables 4 and 5 for the top and bottom laminae, respectively. Goodman corrected cyclic stresses for these laminae are shown in Tables 6 and 7.

As shown in Table 6 the maximum corrected cyclic stress in the top lamina is 36 ksi. This is well below the endurance limit for 17-4 PH steel as shown in Figure 3. Therefore, no damage is predicted for any of the maneuvers for the top lamina.

Table 7 shows that several corrected stresses for the bottom lamina exceed the endurance limit. The resulting damage on the bottom lamina for each of the these maneuvers is shown in Table 8. The damages per maneuver are multiplied by the number of maneuvers per block and summed together to obtain the cumulative block damage also shown in Table 8. This damage is inverted and multiplied by the number hours per block to predict the life in hours for each failure location. As shown in this table, first failure is indicated in the leading throat at 1175 hours for the example spectrum.

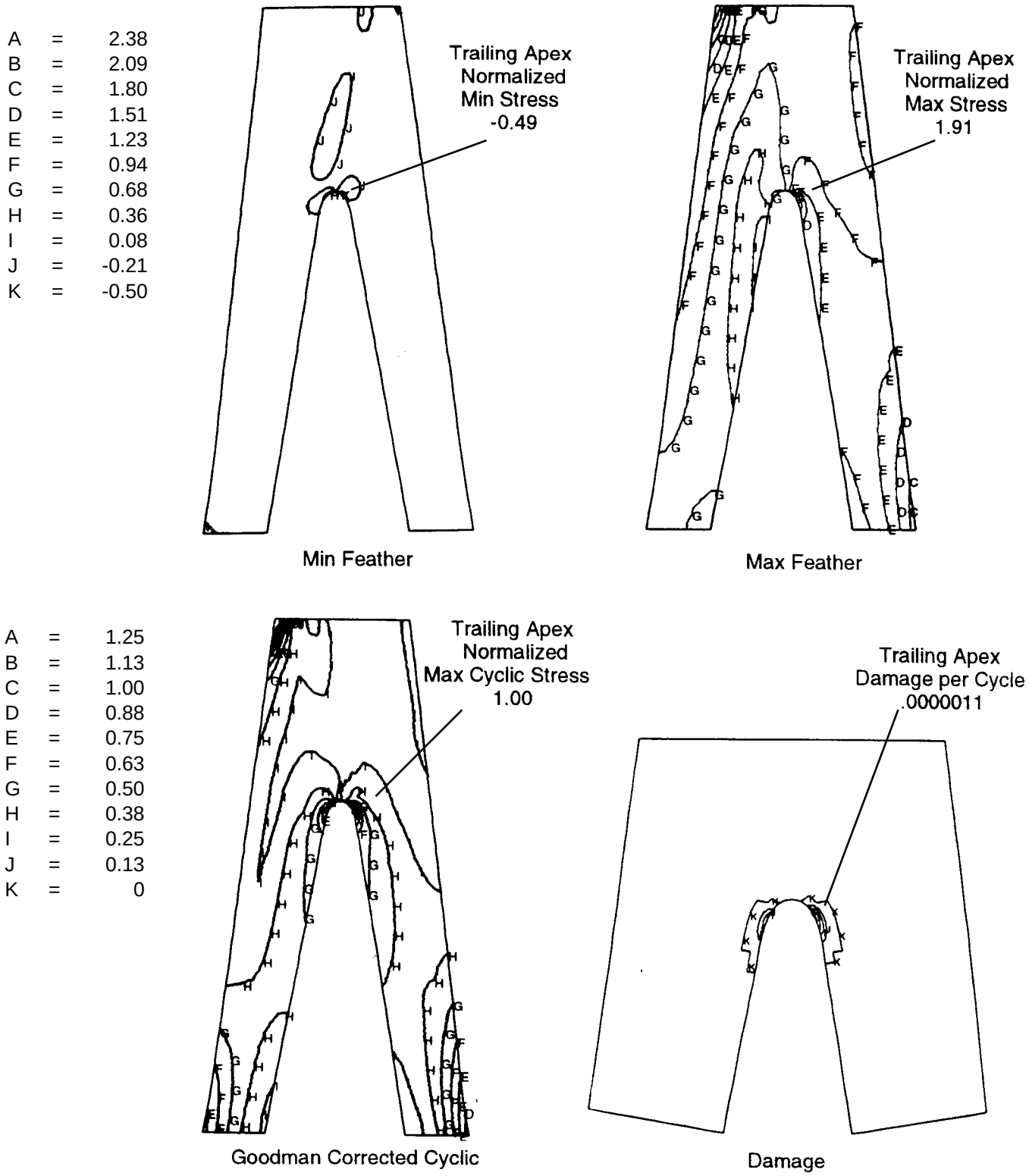

Figure 12. Refined Bottom Lamina Stress Results For Pull Up Maneuver

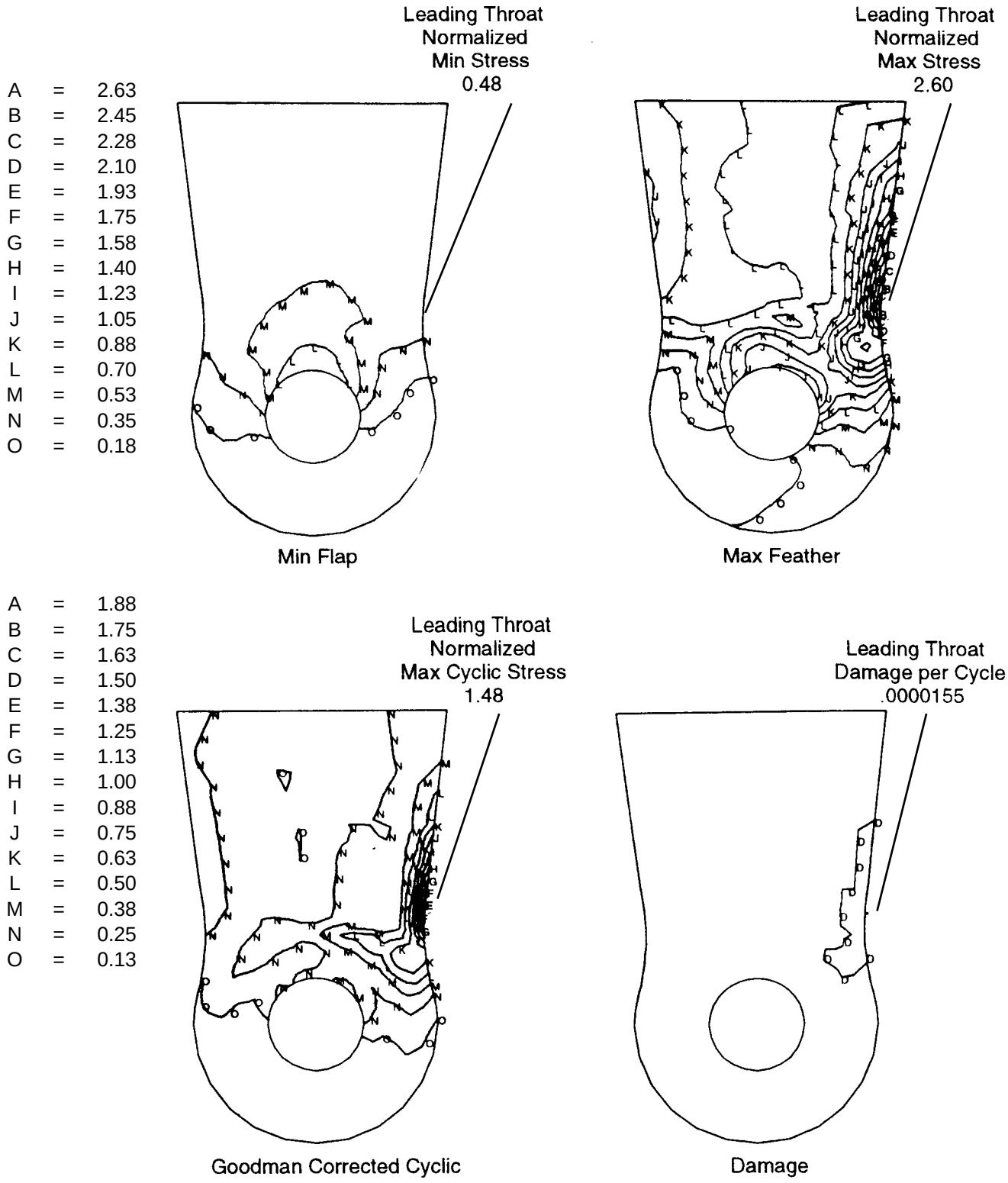

Figure 13. Refined Outboard Bottom Lamina Stress Results For Pull Up Maneuver.

Table 4. Top Lamina Normalized Mean and Cyclic Stress Summary

Maneuver	Apex				Throat				Leg			
	Leading		Trailing		Leading		Trailing		Leading		Trailing	
	mean	cyclic	mean	cyclic	mean	cyclic	mean	cyclic	mean	cyclic	mean	cyclic
Level Flight	0.70	0.40	0.58	0.58	0.14	0.21	0.05	0.25	0.81	0.39	0.00	0.26
Right Turn	0.60	0.43	0.50	0.56	0.25	0.31	0.10	0.28	0.60	0.58	-0.21	0.51
RPO	0.24	0.23	0.31	0.39	0.31	0.45	0.03	0.20	0.50	0.43	-0.36	0.65
Pull Up	0.68	0.29	0.35	0.38	0.13	0.26	0.11	0.28	0.68	0.43	-0.11	0.69

Table 5. Bottom Lamina Normalized Mean and Cyclic Stress Summary

Maneuver	Apex				Throat				Leg			
	Leading		Trailing		Leading		Trailing		Leading		Trailing	
	mean	cyclic	mean	cyclic	mean	cyclic	mean	cyclic	mean	cyclic	mean	cyclic
Level Flight	0.64	0.56	0.48	0.41	1.15	0.34	0.84	0.28	0.98	0.25	0.88	0.31
Right Turn	0.78	0.93	0.68	0.64	1.25	0.31	0.84	0.23	1.10	0.56	0.94	0.53
RPO	0.99	1.15	0.35	1.03	0.85	0.33	0.88	0.49	1.08	0.86	0.75	0.66
Pull Up	0.58	1.20	0.71	1.20	1.54	1.06	0.88	0.40	1.05	0.69	0.96	0.84

Table 6. Top Lamina Normalized Corrected Cyclic Stress Summary

Maneuver	Apex		Throat		Leg	
	Leading	Trailing	Leading	Trailing	Leading	Trailing
	cyclic	cyclic	cyclic	cyclic	cyclic	cyclic
Level Flight	0.33	0.44	0.14	0.16	0.34	0.16
Right Turn	0.34	0.43	0.21	0.18	0.45	0.29
RPO	0.15	0.28	0.31	0.13	0.31	0.35
Pull Up	0.24	0.26	0.18	0.18	0.35	0.40

Table 7. Bottom Lamina Normalized Corrected Cyclic Stress Summary

Maneuver	Apex		Throat		Leg	
	Leading	Trailing	Leading	Trailing	Leading	Trailing
	cyclic	cyclic	cyclic	cyclic	cyclic	cyclic
Level Flight	0.45	0.31	0.36	0.24	0.24	0.28
Right Turn	0.79	0.53	0.36	0.20	0.58	0.49
RPO	1.11	0.73	0.29	0.44	0.86	0.55
Pull Up	0.93	1.00	1.48	0.36	0.68	0.79

Table 8. Bottom Lamina Damage and Life Summary

Maneuver	**Number of Occurrences per 10 hr block**	**Throat**		**Apex**		**Leg**	
		Leading	**Trailing**	**Leading**	**Trailing**	**Leading**	**Trailing**
Level Flight	175000						
Right Turn	7100			.0000001			
RPO	490			.0000026		.0000003	
Pull Up	550	.0000155		.0000006	.0000011		.0000001
Cumulative		.0085095		.0024858	.0006251	.0001440	.0000685
Life (hours)		1175	>1000000	4023	15997	69439	146046

TEST CORRELATION

A laminated metallic stack was fabricated, instrumented with strain gages, and tested to the load points shown in Table 2. A total of 36 strain gages were applied; 18 to each of the upper and lower laminae. Figure 14 shows three gage locations that typically represent high stress locations of the throat, leg, and apex regions of the most highly loaded bottom lamina. These representative locations are used to show the level of correlation between predicted and measured results.

The correlation of the throat and leg as illustrated respectively by Figures 15 and 16 shows excellent agreement between test and analysis. The apex correlation of Figure 17 shows good agreement for the higher strains but poorer correlation at low strain levels. The poor agreement at low strain levels is due to the inability of the analysis to accurately predict buckling wave forms. This disagreement, however, does not greatly effect the calculated life of the LMS. The buckling phenomenon also occurs in the trailing leg of the top lamina under high flap and shear conditions which tend to unload the leg allowing a buckling wave to form. Once again this does not present much of a problem because as was shown in the results section the bottom lamina being more highly loaded will define the first failure location.

In the interest of space only three representative strain gage locations were shown for the correlation. Other strain gage locations exhibit a similar high degree of correlation. This agreement between test and analysis validates the proposed method as a good predictor of LMS behavior.

CONCLUSION

Laminated metallic stacks are efficient systems for carrying all loads required for blade retention while permitting motions necessary for rotorcraft flight. An LMS accomplishes this without the use of bearings that add complexity and weight to the aircraft. The main problem associated with the design of an LMS is that until now accurately analyzing its extreme nonlinear behavior proved to be such a formidable task that it was qualified strictly by costly laboratory and flight test.

A methodology has been presented that provides the means to accurately and efficiently predict the behavior and fatigue life of an LMS. This method which makes use of nonlinear finite element analysis can be used to evaluate a LMS configuration in as little as a few weeks. This will allow the analyst to thoroughly optimize a new design in a reasonable amount of time.

The procedure outlined has been validated by excellent strain correlation between analysis and laboratory results. A representative sample of this correlation has been presented.

REFERENCES

1. Mil Handbook 5D, June 1, 1983, Page 2-164.

2. Mil Handbook 5D, June 1, 1983, Page 2-172.

3. MSC-NASTRAN Version 68.2.3, The MacNeal-Schwendler Corporation, September 11 1995.

4. MSC-PATRAN Release 2.5-5, The MacNeal-Schwendler Corporation.

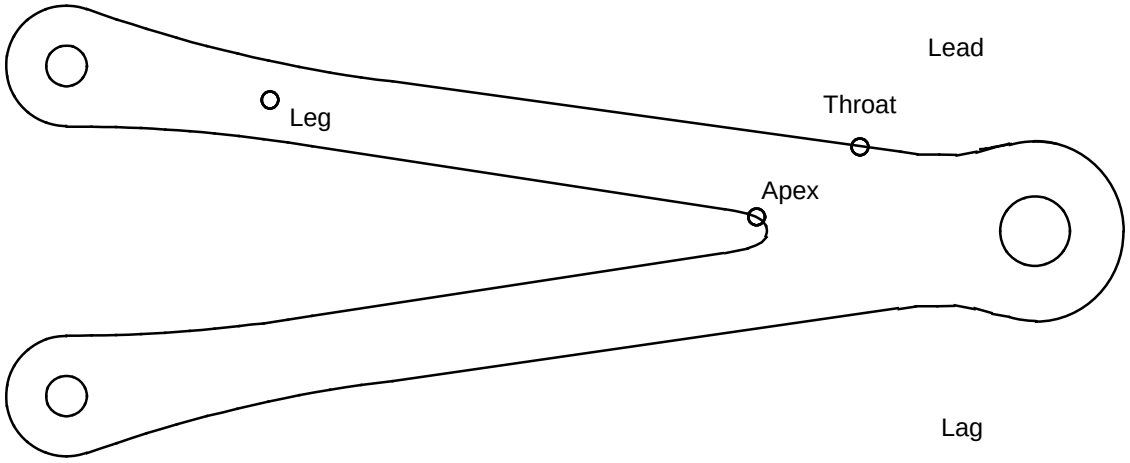

Figure 14. LMS Throat, Apex, and Leg Strain Gage Locations.

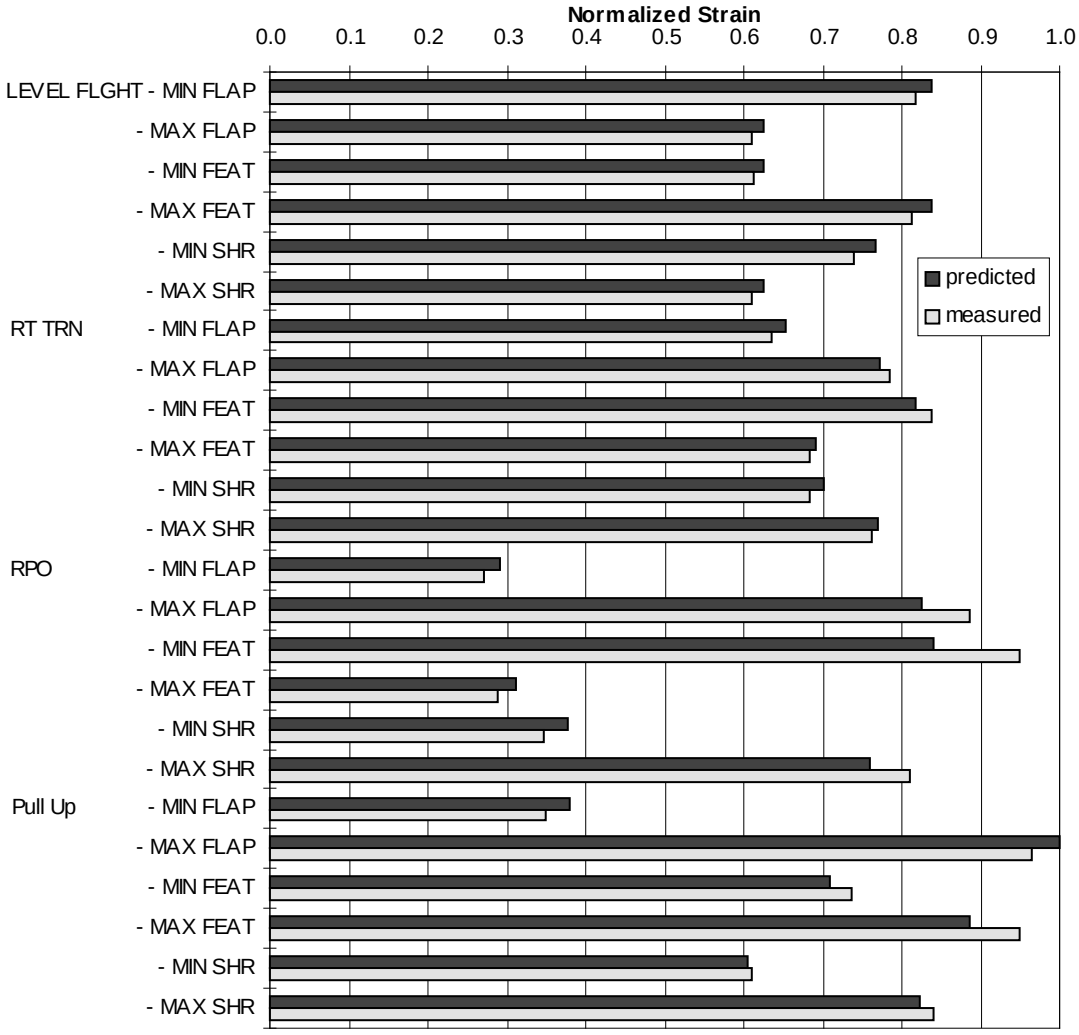

Figure 15. LMS Throat Strain Gage Correlation.

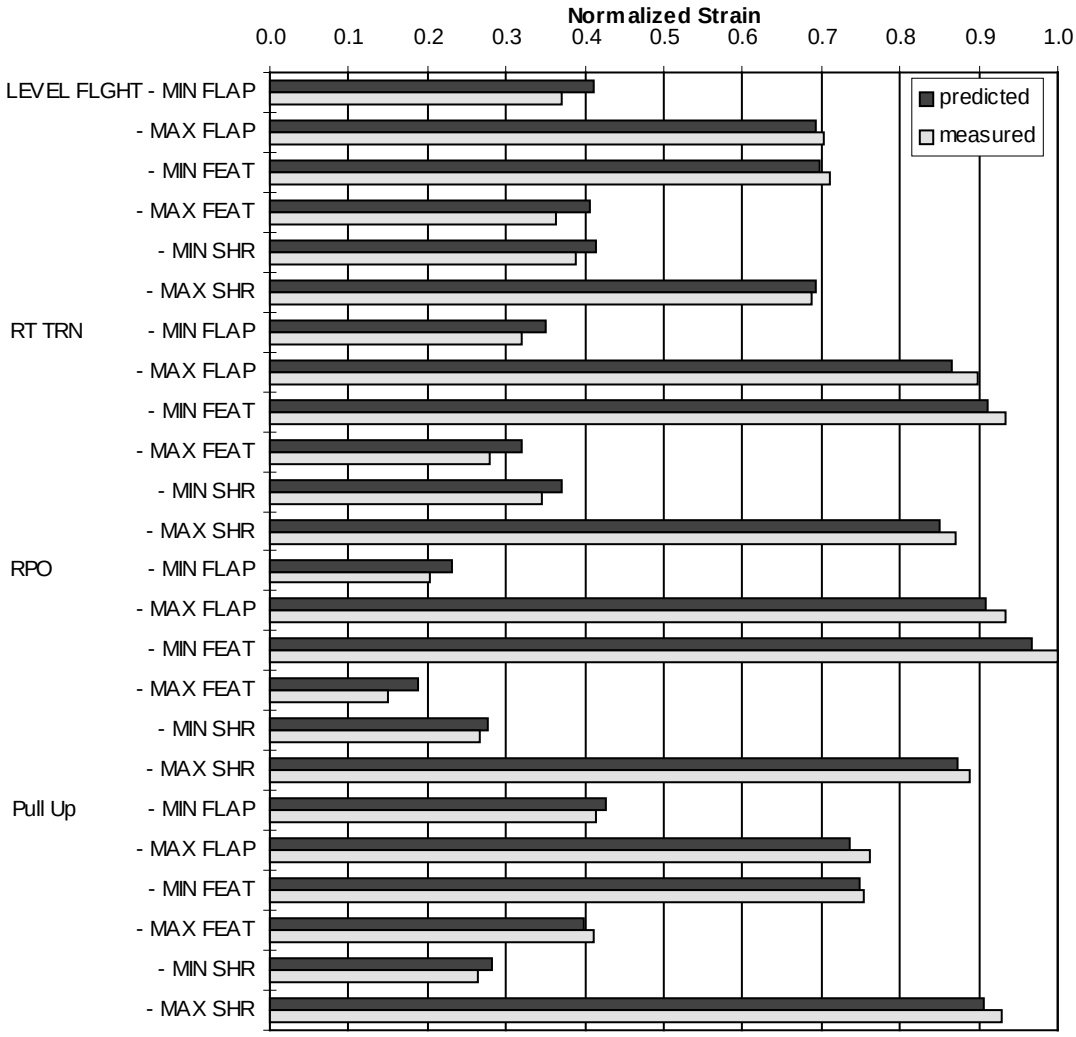

Figure 16. LMS Leg Strain Gage Correlation.

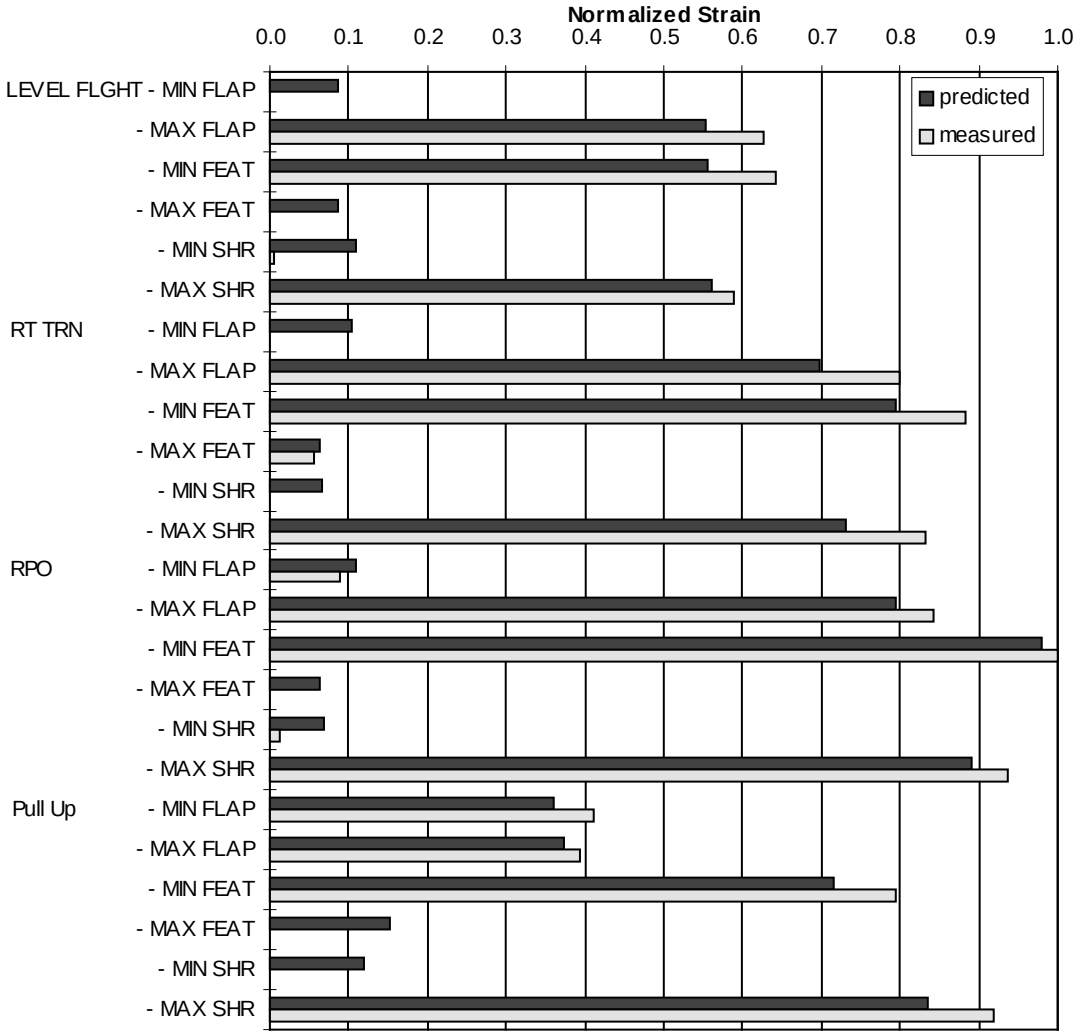

Figure 17. LMS Apex Strain Gage Correlation.